Available on CMS information server

CMS CR -2015/310

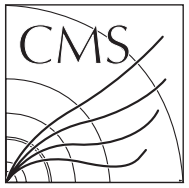

The Compact Muon Solenoid Experiment

Conference Report

Mailing address: CMS CERN, CH-1211 GENEVA 23, Switzerland

19 November 2015

CMS overview

Byungsik Hong for the CMS Collaboration

Abstract

Most recent CMS data related to the high-density QCD are presented for pp and PbPb collisions at 2.76 TeV and pPb collisions at 5.02 TeV. The PbPb collision is essential to understand collective behavior and the final-state effects for the detailed characteristics of hot, dense partonic matter, whereas the pPb collision provides the critical information on the initial-state effects including the modification of the parton distribution function in cold nuclei. This paper highlights some of recent heavy-ion related results from CMS.

Presented at *QM2015 Quark Matter 2015, XXV INTERNATIONAL CONFERENCE ON ULTRA-RELATIVISTIC NUCLEUS-NUCLEUS COLLISIONS*

Available online at www.sciencedirect.com
ScienceDirect
Nuclear Physics A 00 (2015) 1–8
Nuclear Physics A
www.elsevier.com/locate/procedia

Overview of recent heavy-ion results from CMS

Byungsik Hong (for the CMS Collaboration)[1]

Department of Physics, Korea University, Seoul 02841, Republic of Korea

Abstract

Most recent CMS data related to the high-density QCD are presented for pp and PbPb collisions at 2.76 TeV and pPb collisions at 5.02 TeV. The PbPb collision is essential to understand collective behavior and the final-state effects for the detailed characteristics of hot, dense partonic matter, whereas the pPb collision provides the critical information on the initial-state effects including the modification of the parton distribution function in cold nuclei. This paper highlights some of recent heavy-ion related results from CMS.

Keywords: CMS, QCD, quark-gluon plasma, collectivity, fluctuation, jet, heavy flavor, quarkonium, Z

1. Introduction

Since 2010 the Compact Muon Solenoid (CMS) Collaboration at the Large Hadron Collider (LHC) has recorded total ~5.6 pb^{-1} pp and ~160 μb^{-1} PbPb collisions at $\sqrt{s_{NN}}$ = 2.76 TeV and ~35 nb^{-1} pPb collisions at 5.02 TeV. The PbPb data are important to investigate the detailed characteristics of the high-density partonic matter and the final-state effects, such as collective behavior and jet quenching, by comparing to the pp reference data. On the other hand, the asymmetric pPb data are essential to study the initial-state effects such as the nuclear parton distribution function (nPDF), multiple collisions, and initial energy loss. CMS also analyzed the low pile-up pp data at 7 and 13 TeV in order to elucidate the energy dependence of the global observables and the origin of collectivity and fluctuation. In following, the most recent pp, pPb, and PbPb data from CMS are summarized. All heavy-ion related data are available in the public website [1].

[1] A list of members of the CMS Collaboration and acknowledgements can be found at the end of this issue.

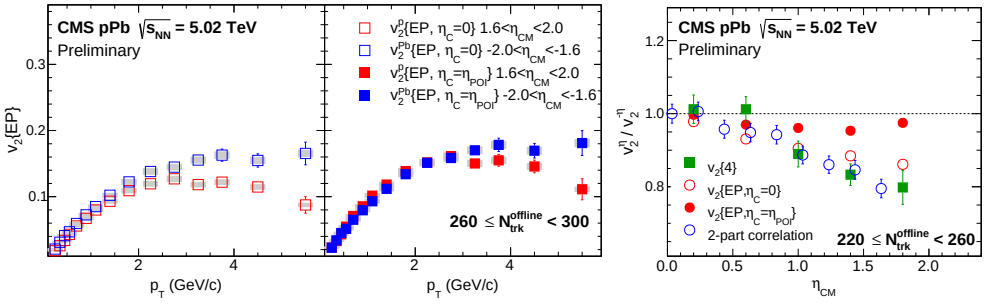

Fig. 1. (Left) Comparison of $v_2\{EP\}$ distributions as a function of p_T for the event plane (EP) reconstructed by HF on the p-going ($v_2^{\rm p}$) and Pb-going ($v_2^{\rm Pb}$) sides for high-multiplicity pPb events [6]. The left and middle panels are for $\eta_C = 0$ and η_{POI}, respectively. (Right) Ratio of $v_2^{\rm p}/v_2^{\rm Pb}$ at comparable center-of-mass pseudorapidity η_{CM} in pPb. The filled circles represent the $v_2\{EP\}$ data after correcting the EP decorrelation effect. For comparison the data from 2- and 4-particle correlations are also displayed.

2. Global observable, collectivity and fluctuation

The pseudorapidity η distributions of charged hadrons in pp at 13 TeV was analyzed by CMS [2]. The averaged pseudorapidity density $dN_{ch}/d\eta$ in $|\eta| < 0.5$ is 5.49 ± 0.01(stat) ± 0.17(syst) for inelastic events. The beam-energy dependence of inelastic $dN_{ch}/d\eta$ from ISR to CMS can be empirically fitted by a second-order polynomial in ln(s), where s in GeV^2, which provides new constraint for various QCD aspects of hadronic event generators.

The centrality and η dependences of the transverse-energy (E_T) flow in pPb at 5.02 TeV was also analyzed [3]. For minimum bias events $dE_T/d\eta$ at midrapidity reaches about 23 GeV, which is comparable to that in peripheral (70 - 80%) PbPb at 2.76 TeV [4]. The local energy density in minimum bias pPb is estimated to be about one half of that in the most central (0 - 2.5%) PbPb collisions.

Previously, CMS revealed the collective nature of multiparticle correlations in high-multiplicity pPb events at 5.02 TeV [5]. However, the ambiguity in interpretation still remains open as the initial-state effect due to the gluon saturation may also describe the data. In order to shed more lights on the underlying mechanism, the η and p_T dependences of the azimuthal-flow harmonics (v_n) was analyzed for pPb [6]. In particular, a different momentum-dependent event-plane (EP) decorrelation on the p- and Pb-going sides are carefully analyzed by employing the η window of the particle of interest ($\eta_C = \eta_{POI}$), instead of the midrapidity window ($\eta_C = 0$), in determining the third subevent angle for the EP-resolution-correction factors.

Figure 1 shows the p_T dependences of $v_2\{EP\}$ when the event planes are reconstructed by using the hadronic forward (HF) calorimeter ($2.9 < |\eta| < 5.2$) on the p-going ($v_2^{\rm p}$) and Pb-going ($v_2^{\rm Pb}$) sides in pPb with offline track multiplicity $N_{trk}^{offline}$ between 260 and 300. The v_2 on the Pb-going side is similar to that on the p-going side at low p_T but enhanced at high p_T. The difference is reduced when the EP decorrelation is corrected. The right panel of Fig. 1 shows the ratios of the yield weighted and integrated v_2 values on the p- and Pb-going sides as a function of comparable center-of-mass pseudorapidity η_{CM} for pPb. The pseudorapidity dependent asymmetry of $v_2^{\rm p}/v_2^{\rm Pb}$ is significantly reduced when the EP decorrelation effects are taken into account.

Having assumed that the event-plane angle is global for all particles of the entire event, the long-range azimuthal two-particle Fourier harmonics were used to be factorized into a product

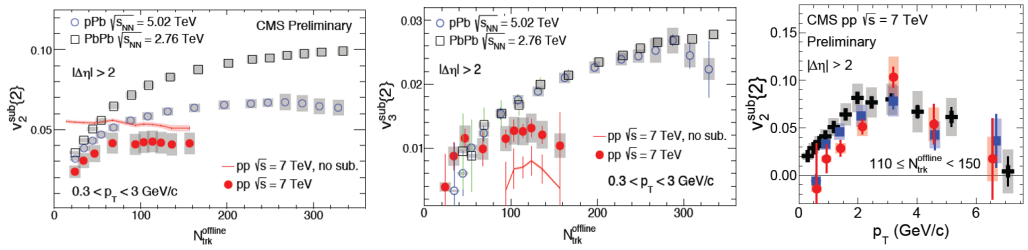

Fig. 2. $v_2^{sub}\{2\}$ (left) and $v_3^{sub}\{2\}$ (center) of charged particles averaged over $0.3 < p_T < 3$ GeV/c as a function of N_{trk}^{offine} in pp at 7 TeV, pPb at 5.02 TeV and PbPb at 2.76 TeV [9]. The superscript "sub" means that back-to-back jet correlations are estimated from low-multiplicity ($10 \leq N_{trk}^{offine} < 20$) pp events and subtracted. The results without correcting the jet correlations in pp are shown as solid lines. The right panel shows the $v_2^{sub}\{2\}$ distributions of inclusive charged particles, K_S^0, and $\Lambda/\bar{\Lambda}$ as a function of p_T in high multiplicity ($110 \leq N_{trk}^{offine} < 150$) pp events at 7 TeV. The shaded areas represent the systematic uncertainties for all panels.

of single-particle anisotropic harmonics. However, a significant factorization breakdown of v_2, up to about 20%, were observed for particle pairs in ultra-central (0 - 0.2%) PbPb, which hinted sizable fluctuations in the initial geometry of two nuclei [7]. CMS employed the principal component analysis (PCA) to extract the leading and subleading flow modes for pPb and PbPb [8]. The leading v_2 modes essentially agree with the values obtained by the standard elliptic-flow analysis. The subleading v_2 modes, reflecting the amount fluctuation, are close to zero at low p_T with slight increases towards high p_T for both systems. In p_T = 1.7 - 2.7 GeV/c, where the factorization breakdown effect is largest in high-multiplicity pPb, the subleading v_2 modes show a significant non-zero magnitude due to the strong non-flow presence. The subleading v_3 modes are practically 0 up to 2 GeV/c for pPb and PbPb.

CMS also analyzed the long-range 2- and 4-particle angular correlations in pp at 7 TeV as a function of N_{trk}^{offine} [9]. The high-multiplicity pp events show a long-range ($|\Delta\eta| > 2$), near-side ($|\Delta\phi| \sim 0$) structure (the so-called "ridge") in the 2-particle correlation functions. Figure 2 shows the v_2 and v_3 distributions of charged particles averaged over $0.3 < p_T < 3$ GeV/c from 2-particle correlations. The back-to-back jet correlation components are estimated from low-multiplicity ($10 \leq N_{trk}^{offine} < 20$) pp events and subtracted. For comparison the results of pPb at 5.02 TeV [10] and PbPb at 2.76 TeV [11] are also shown. In general, the v_2^{sub} values in pp are smaller than those in pPb, which are, subsequently, smaller than those in PbPb over a wide multiplicity range. This observation is consistent with the elliptic flow phenomenon in a hydrodynamic picture that is sensitive to the initial-state collision geometry. In contrast the v_3^{sub} values for $N_{trk}^{offine} < 90$ are comparable to those in pPb and PbPb within the uncertainties.

The right panel of Fig. 2 shows the v_2^{sub} data of inclusive charged particles (mostly $\pi^{\pm}$), K_S^0, and $\Lambda/\bar{\Lambda}$ extracted from long-range 2-particle correlations for high-multiplicity ($110 \leq N_{trk}^{offine} <$ 150) pp. In $p_T < 2.5$ GeV/c, the mass ordering effect, having observed in pPb and PbPb, is also visible in high-multiplicity pp: the lighter hadron species exhibit a stronger v_2^{sub} signal, which is consistent with a hydrodynamic picture. However, for $p_T > 2.5$ GeV/c, the v_2 values of the three particle species are identical within uncertainties, and approach to zero at $p_T \geq 6$ GeV/c.

The strange hadrons (K_S^0, $\Lambda/\bar{\Lambda}$, $\Xi^{\pm}$) were exclusively reconstructed and analyzed as a function of p_T over a wide range of event multiplicity and rapidity in pp, pPb, and PbPb [12]. The p_T spectra are flatter toward higher $N_{trk}^{offline}$ for all systems, and heavier particles show flatter spectra

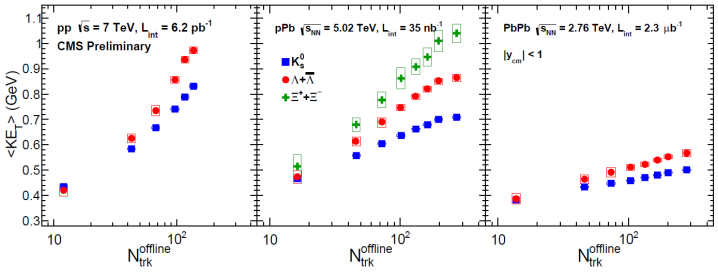

Fig. 3. Average transverse kinetic energy $\langle KE_T \rangle$ near midrapidity ($|y_{\rm cm}| < 1$) for K^0_S, $\Lambda/\bar{\Lambda}$, and $\Xi^{\pm}$ as a function of event multiplicity $N^{offline}_{trk}$ in pp (left), pPb (center) and PbPb (right) collisions [12]. The error bars and boxes represent the statistical and systematic uncertainties, respectively.

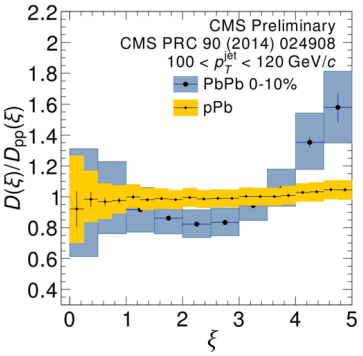

Fig. 4. Ratio of the fragmentation function in pPb, $D_{\rm pPb}$, and the interpolated pp reference, $D_{\rm pp}$, as a function of $\xi = \log(p^{jet}/p^{track}_{\parallel})$, where $p^{track}_{\parallel}$ is the tracks momentum parallel to the jet axis [13]. The pp reference is constructed by using the interpolation of existing data at 2.76 and 7 TeV considering the expected flavor mixture at 5.02 TeV from PYTHIA. For comparison the fragmentation function in PbPb is also displayed. Underlying events are subtracted by using a 90-degree rotated cone in ϕ direction.

than lighter ones within a collision system. Figure 3 summarizes the average transverse kinetic energy $\langle KE_T \rangle = \langle m_T \rangle - m$, where $m_T = \sqrt{p_T^2 + m^2}$ is the transverse mass with m the rest mass, as a function of $N^{offline}_{trk}$. In each collision system the $\langle KE_T \rangle$ values at the lowest $N^{offline}_{trk}$ bin for each particle species are similar, consistent with the m_T-scaling phenomenon. As event multiplicity increases, the $\langle KE_T \rangle$ values monotonically increase with $N^{offline}_{trk}$ for all particle species. The m_T scaling is broken as the $\langle KE_T \rangle$ values of heavier particle species increase faster with $N^{offline}_{trk}$ for all systems. The separation among different particle species in $\langle KE_T \rangle$ is larger for high-multiplicity pp and pPb events than for PbPb events.

3. Jet

The jet fragmentation function was extracted in pPb at 5.02 TeV [13]. Because no pp data are available at this energy, the pp reference is constructed by interpolating between the available 2.76 and 7 TeV data. Figure 4 shows the ratio of the pPb fragmentation function $D_{\rm pPb}$ and the interpolated pp reference $D_{\rm pp}$ as a function of $\xi = \log(p^{jet}/p^{track}_{\parallel})$, where $p^{track}_{\parallel}$ is the tracks momentum parallel to the jet axis. The jet fragmentation function in pPb is similar to that in pp as $D_{\rm pPb}(\xi)/D_{\rm pp}(\xi)$ is consistent with unity. Therefore, a significant enhancement of the low-p_T jet tracks observed in PbPb can be attributed to the final-state effect with absence of any modifications in $D_{\rm pPb}$ and R_{pA}, nuclear modification factor, of jet in pPb.

To understand the details of the energy-loss phenomenon of partons propagating in hot, dense medium, the momentum flow in PbPb and pp containing high momentum jets was analyzed.

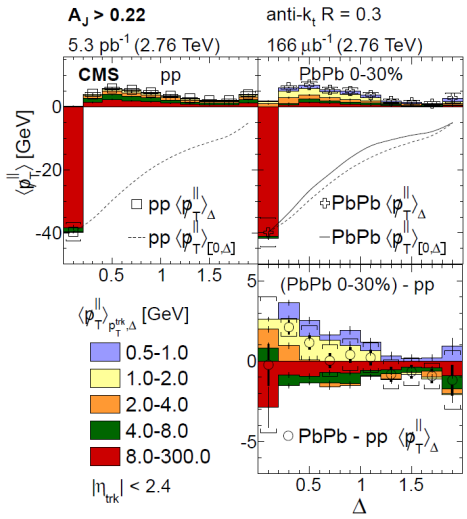

Fig. 5. (Upper) Differential missing p_T distributions for pp and central (0 - 30%) PbPb in various p_T ranges, indicated by different colors, as a function of relative angle $\Delta = \sqrt{(\eta_{trk} - \eta_{jet})^2 + (\phi_{trk} - \phi_{jet})^2}$ [15]. The total integrated missing p_T for a given Δ bin, $\langle \not{p}_T^{\parallel} \rangle$, are displayed by open squares and crosses for pp and PbPb, respectively. The dashed and solid lines show the cumulative $\langle \not{p}_T^{\parallel} \rangle$, i.e., the total $\langle \not{p}_T^{\parallel} \rangle$ over Δ starting from $\Delta = 0$, for pp and central PbPb, respectively. (Lower) Difference between the central PbPb and pp differential $\langle \not{p}_T^{\parallel} \rangle$ distributions per p_T range (colored boxes). The difference of the total $\langle \not{p}_T^{\parallel} \rangle$ values between central PbPb and pp are shown by open circles as a function of Δ. The error bars and brackets represent the statistical and systematic uncertainties, respectively. All displayed data are for the p_T imbalanced dijet events with $A_J > 0.22$.

Compared to pp, an increase in the fraction of dijet events with large p_T asymmetry $A_J = (p_{T,1} - p_{T,2})/(p_{T,1} + p_{T,2})$ between the leading and subleading jets was observed in central PbPb, which is consistent with the pathlength-dependent differential energy loss [14]. The overall energy balance can be restored when low-momentum particles with $p_T < 2$ GeV/c at large angles beyond the jet boundary are included. The momentum distribution of the excess energy in asymmetric dijet events in PbPb is much softer than that in pp, where the momentum balance is typically carried by a third semi-hard jet.

For the angular radiation pattern in dijet events, the azimuthal angle is divided into the near-side leading and the away-side subleading jet hemispheres [15, 16, 17]. For each event, the projection of p_T of the reconstructed charged particles onto an axis in the dijet azimuthal plane (ϕ_{Dijet}) midway between the leading and subleading jet directions is estimated, and the missing p_T component $\not{p}_T^{\parallel} = \sum_i [-p_T^i \cos(\phi_i - \phi_{Dijet})]$, where i runs over tracks, is determined. By definition $\not{p}_T^{\parallel}$ is positive (negative) for an excess in the direction of the subleading (leading) jet dierction. For pp and peripheral PbPb, the excess of high p_T particles in the direction of the leading jet is mostly balanced by intermediate p_T = 2 - 8 GeV/c particles in the direction of subleading jet. For more central PbPb, the balancing contribution is shifted from the intermediate to low-p_T (= 0.5 - 2 GeV/c) region.

For the angular distribution of the energy loss relative to the dijet axis the contribution to the overall $\langle \not{p}_T^{\parallel} \rangle$ values in annular regions around the leading and subleading jet axes are extracted. Figure 5 shows $\langle \not{p}_T^{\parallel} \rangle$ for pp and central (0 - 30%) PbPb in various p_T ranges as a function of relative angle $\Delta = \sqrt{(\eta_{trk} - \eta_{jet})^2 + (\phi_{trk} - \phi_{jet})^2}$. A large $\langle \not{p}_T^{\parallel} \rangle$ contribution from high-p_T particles towards the leading-jet hemisphere in small Δ (< 0.2) is balanced by the contribution from low-p_T particles towards the subleading-jet hemisphere in larger Δ (> 0.2) for central PbPb, as manifested by the lower panel of Fig. 5 for the difference between central PbPb and pp. This observation suggests an additional mechanism for asymmetric dijet production, such as parton energy loss traversing in medium, in PbPb.

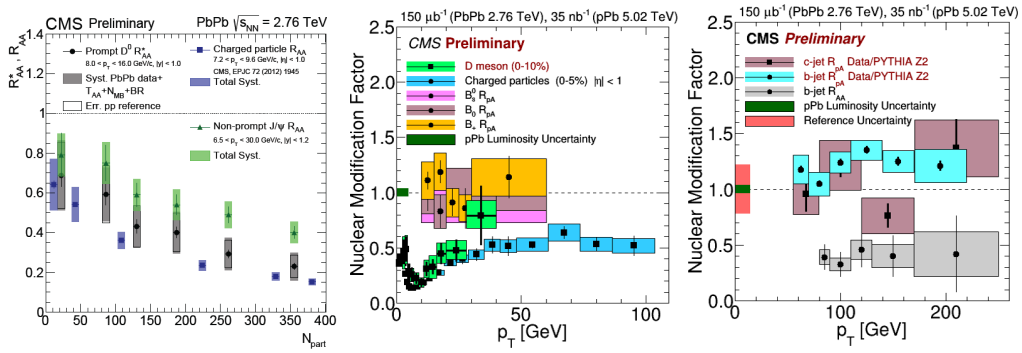

Fig. 6. (Left) Nuclear modification factor R^*_{AA} of D^0 for $8 < p_T < 16$ GeV/c in $|y| < 1$ (circles) as a function of the estimated number of participant nucleons N_{part} in PbPb [18]. (The superscript $*$ indicates that the pp reference used in this analysis is derived from a FONLL calculation and the extrapolated pp data at 7 TeV from ALICE.) The R_{AA}'s for non-prompt J/ψ from B-meson decay (upper most triangles) and charged particles (lowest squares) are also shown for comparison. (Center) The R_{AA} distributions of D^0 and charged hadrons [22] as a function of p_T for central PbPb. The R_{pA} data around 0 represent the $B^{\pm}$, B^0 and B^0_s data in pPb for comparison [23]. (Right) The R_{pA} distributions of c and b jets in pPb as a function of p_T [24, 25]. The R_{AA} of b jet in central (0 - 10%) PbPb are also displayed for comparison [26]. The shaded boxes at $p_T = 0$ in the middle and right panels represent the systematic uncertainties from pPb luminosity and pp references. In the prompt D^0 spectra, D^0s from B decays are subtracted using the FONLL calculations.

4. Open heavy flavor, quarkonium and electroweak boson

Heavy c and b quarks are produced primarily in early stage of heavy-ion collisions due to their large masses. Compared to light quarks and gluons, they are expected to lose less energy while traversing the medium because of color charge and the dead cone effect. Thus, the experimental data on the heavy-flavor production are crucial to reveal the properties of the strongly interacting QCD matter. CMS analyzed the nuclear modification factor R^*_{AA} of prompt D^0 as functions of p_T and collision centrality in PbPb [18], where the superscript $*$ represents the pp reference does not come from the measurement, but derived from a fixed-order next-to-leading logarithm (FONLL) calculations [19] and the extrapolated pp data at 7 TeV from ALICE [20].

The left panel of Fig. 6 shows the centrality dependence of R^*_{AA} for prompt D^0 ($8.0 < p_T < 16.0$ GeV/c in $|y| < 1.0$) compared to the R_{AA}'s for non-prompt J/ψ from B-meson decay [21] and charged particles [22]. The R^*_{AA} of prompt D^0 is suppressed from semi-central to central PbPb, and lies in between the charged particles and non-prompt J/ψ data. The p_T dependence of R^*_{AA} for prompt D^0 in central (0 - 10%) PbPb is shown in the middle panel of Fig. 6. It shows a clear trend of smaller suppression towards higher p_T. The figure also displays the R_{pA} distributions of exclusively reconstructed $B^{\pm}$, B^0, and B^0_s mesons in pPb [23]. In contrast to the R^*_{AA} of prompt D^0 in PbPb, the R_{pA}'s of B mesons are not suppressed within the current uncertainties. The right panel of Fig. 6 shows the first measurement of R_{pA} of c-jet in pPb [24] together with those of b jet in pPb [25] and central (0 - 10%) PbPb [26] as a function of p_T. The p_T spectra of c and b jets in pPb are consistent with PYTHIA simulation. Differently R_{AA} of b jet in central PbPb is about 0.4 in $p_T > 80$ GeV/c for the central (0 - 10%) PbPb.

The left and middle panels of Fig. 7 show the forward-to-backward yield ratios R_{FB} of prompt J/ψ in three different rapidity ranges in pPb as functions of p_T and the event activity variable, defined by E_T measured in HF in $4 < |\eta| < 5.2$, respectively [27]. R_{FB} decreases monotonically towards smaller p_T and larger $E_T^{HF|\eta|>4}$ without any strong rapidity dependence. The prompt

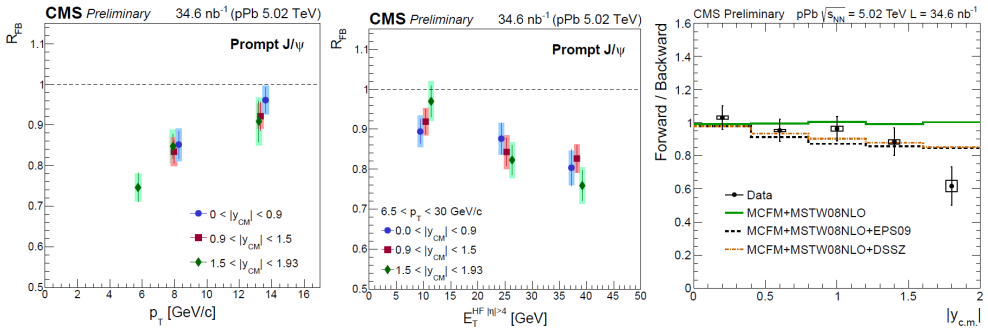

Fig. 7. Forward-to-backward yield ratio R_{FB} of prompt J/ψ in three different rapidity ranges in pPb as functions of p_T (left) and $E_T^{HF|\eta|>4}$, measured by HF in $4 < |\eta| < 5.2$ (center) [27]. The right panel shows R_{FB} of Z bosons in pPb as a function of the center-of-mass rapidity for the combined leptonic decay channels ($\mu^-\mu^+$ and e^-e^+) [28]. The data are compared to the model calculations using MCFM generators. The error bars and boxes show the statistical and systematic uncertainties, respectively.

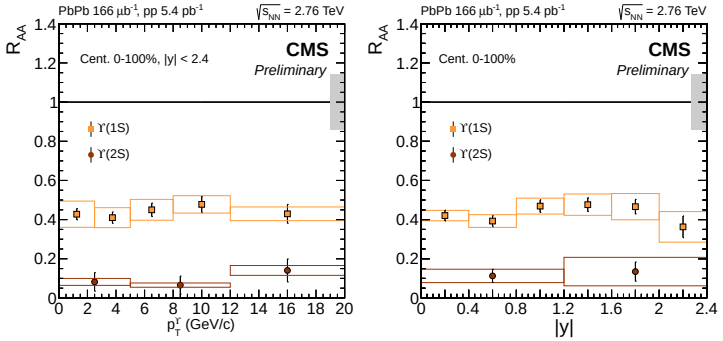

Fig. 8. R_{AA} of Υ(1S) and Υ(2S) in PbPb as a function of p_T (left) and y (right) [29]. The error bars and boxes represent the statistical and systematic uncertainties, respectively. The box at unity represents the global fully-correlated uncertainty.

(and also non-prompt, not shown here) J/ψ yields at forward rapidities are smaller than those at backward rapidities, with a strong dependence on the event activity. This observation implies the presence of cold nuclear-matter effects in a smaller momentum fraction (Bjorken x) region in the Pb nucleus.

The right panel of Fig. 7 shows the forward-to-backward yield ratio of Z bosons for combined leptonic decay channels of both $\mu^-\mu^+$ and e^-e^+, in pPb as a function of the center-of-mass rapidity [28]. The experimental data are compared to the MCFM calculations with and without the nuclear modification from EPS09 or DSSZ nPDF sets. The data prefer the presence of nuclear effects in PDFs, which provides an important contraint to the nPDF uncertainties.

The improved data on R_{AA}'s of Υ(1S) and Υ(2S) in PbPb are shown in Fig. 8 as a function of p_T and rapidity [29]. The new data include ~30% more statistics for Υ(1S) in PbPb and fully analyzed pp reference events recorded in 2013. The R_{AA} values, integrated over p_T and rapidity, are $0.425 \pm 0.029(\text{stat}) \pm 0.070(\text{syst})$ for Υ(1S) and $0.116 \pm 0.028(\text{stat}) \pm 0.022(\text{syst})$ for Υ(2S). Υ(3S) cannot be identified in PbPb, and only upper limit of 0.14 is given at 95% confidence level. Interestingly enough the R_{AA} distributions are constant within uncertainties as a function of both p_T and rapidity, and no pronounced dependence on the kinematic variables is observed.

5. Summary

Since the last Quark Matter Conference (QM2014), the CMS Collaboration has obtained various new results on the collective behavior, fluctuations, jets, open and closed heavy flavors, and electroweak bosons. The local energy density in pPb is compatible to that in PbPb from the E_T-flow analysis. The flow-like phenomena are observed not only in large systems like PbPb, but also in high-multiplicity pp and pPb collisions.

The jet fragmentation functions are measured to be similar for both pp and pPb. A large missing p_T contribution from high-p_T particles towards the leading-jet hemisphere in small angles is balanced by the contribution from low-p_T particles towards the subleading-jet hemisphere in larger angles in central PbPb.

The nuclear modification factors of prompt D^0 is suppressed less than charged particles but more than non-prompt J/ψ from B decay, which is in accord with the predicted dead cone effect. The J/ψ and Z yields in pPb prefer the modified parton distribution functions in Pb nucleus. Finally, the R_{AA} distributions of Υ(1S) and Υ(2S) in PbPb do not show any p_T and rapidity dependences, which cannot be described by models.

References

[1] CMS Collaboration, https://twiki.cern.ch/twiki/bin/view/CMSPublic/PhysicsResultsHIN .
[2] CMS Collaboration, "Pseudorapidity distribution of charged hadrons in proton-proton collisions at $\sqrt{s}$ = 13 TeV", arXiv:1507.05915, CMS PAS FSQ-15-001, submitted to Phys. Lett. B.
[3] M. Murray for CMS Collaboration, these proceedings.
[4] CMS Collaboration, "Measurement of the pseudorapidity and centrality dependence of $dE_T/d\eta$ in PbPb collisions at $\sqrt{s_{NN}}$ = 2.76 TeV extending into the very forward phase-space", CMS PAS HIN-12-006.
[5] CMS Collaboration, Phys. Rev. Lett. 115 (2015) 012301.
[6] Q. Wang for CMS Collaboration, these proceedings.
[7] CMS Collaboration, Phys. Rev. C 92 (2015) 034911.
[8] J. Milocevic for CMS Collaboration, these proceedings.
[9] Z. Chen for CMS Collaboration, these proceedings.
[10] CMS Collaboration, Phys. Lett. B 724 (2013) 213.
[11] CMS Collaboration, J. High Energy Phys. 02 (2014) 088.
[12] H. Ni for CMS Collaboration, these proceedings.
[13] A. Baty for CMS Collaboration, these proceedings.
[14] CMS Collaboration, Phys. Rev. C 84 (2011) 024906.
[15] C. McGinn for CMS Collaboration, these proceedings.
[16] O. Evdokimov for CMS Collaboration, these proceedings.
[17] CMS Collaboration, "Jet-track correlation functions in PbPb collisions", CMS PAS HIN-14-016.
[18] J. Sun for CMS Collaboration, these proceedings.
[19] M. Cacciari, M. Greco, and P. Nason, J. High Energy Phys. 007, 9805 (1998).
[20] ALICE Collaboration, J. High Energy Phys. 1201 (2012) 128.
[21] CMS Collaboration, "Prompt and non-prompt J/ψ R_{AA} with 150 μb^{-1} integrated PbPb luminosity at $\sqrt{s_{NN}}$ = 2.76 TeV", CMS PAS HIN-12-014.
[22] CMS Collaboration, Eur. Phys. J. C 72 (2012) 1945.
[23] CMS Collaboration, "Study of B meson production in pPb collisions at $\sqrt{s}$ = 5.02 TeV using exclusive hadronic decays", arXiv:1508.06678, CMS PAS HIN-14-004, submitted to Phys. Rev. Lett.
[24] CMS Collaboration, "Charm-tagged jet production in pPb collisions at 5.02 TeV and pp collisions at 2.76 TeV", CMS PAS HIN-15-012.
[25] CMS Collaboration, "Transverse momentum spectra of b jets in pPb collisions at $\sqrt{s}$ = 5.02 TeV", arXiv:1510.03373, CMS PAS HIN-14-007, submitted to Phys. Lett. B.
[26] CMS Collaboration, Phys. Rev. Lett. 113 (2014) 132301.
[27] Y. Kim for CMS Collaboration, these proceedings.
[28] E. Chapon for CMS Collaboration, these proceedings.
[29] M. Jo for CMS Collaboration, these proceedings.